Is Driver on Phone Call? Mobile Device Localization using Cellular Signal

Shichen Zhang, *Student Member, IEEE,* Huacheng Zeng, *Senior Member, IEEE,* Y. Thomas Hou, *Fellow, IEEE*

***Abstract*—The use of mobile phones while driving is a major source of distraction for vehicle drivers and has resulted in a large number of car accidents. While surveillance cameras can be used to detect the violation of phone use, they do not work well in some scenarios (e.g., darkness and blockage) and may raise privacy concerns. In this paper, we present PhoLoc, a roadside device to detect the violation of phone use in personal vehicles using the cellular signals emitted by cellphones. PhoLoc is equipped with two sensors: a multi-antenna radio receiver and a low-cost lidar. It jointly processes the multimodal data from the two sensors to estimate the *relative* location of a phone in a vehicle. The enabler of PhoLoc is a new near-field localization scheme, which is capable of estimating the location of a moving phone at a specific time moment by overhearing its cellular signals. We have built a prototype of PhoLoc and evaluated its performance in realistic scenarios. Experimental results show that PhoLoc achieves 4.2% false positive rate and 13.8% false negative rate in the detection of phone call violation.**

***Index Terms*—Positioning over cellar networks, wireless localization, violation of phone use, transportation safety**

I. Introduction

According to the study carried out by the National Highway Traffic Safety Administration (NHTSA), the prevalence of drivers using mobile phones is the main cause of 553,000 property damage crashes, 248,000 injuries, 3,211 fatalities in U.S. in 2021 [1]. Many countries and areas (e.g., UK, Europe, and China) have legislated laws that prohibit vehicle drivers from using mobile phones while driving. Roadside transportation infrastructure that can enforce the laws and alert distracted drivers is critical to improve the safety of driving. A natural approach is to deploy high-resolution surveillance cameras on the roadside to detect drivers' violations of phone use [2]. However, camera surveillance systems may not work well in some scenarios such as darkness, bad weather conditions, or driver's intentional hiding of his/her phone device. More importantly, camera surveillance in public areas may raise serious concerns about the privacy of drivers and passengers.

The limitations and concerns of camera-based surveillance systems in transportation have spurred research efforts that explore alternatives for detecting driver's phone use violations. For example, smartphone sensors such as Global Positioning System (GPS) and Inertial Measurement Unit (IMU) have been studied to detect distracted driving behaviors in an increasing sophisticated manner [3], [4], [5], [6], [7], [8], [9]. In-vehicle Radio Frequency Identification (RFID) based sensing systems have also been developed to detect drivers' distractive driving behaviors [10], [11], [12]. However, both IMU and RFID sensors can only be used *inside* vehicles but cannot be deployed on roadsides to enforce safety regulations. It is desirable to have a *roadside* sensor that can detect the violation of phone use while performing well in all weather conditions and respecting drivers' privacy.

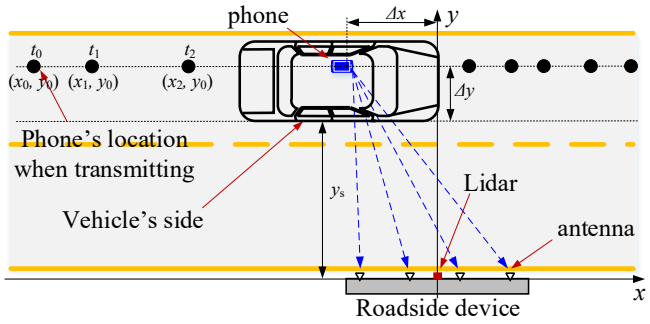

Fig. 1: Illustration of PhoLoc.

In this paper, we present PhoLoc, a roadside device that detects driver's violation of phone use (being on a phone call while driving) in personal vehicles. Fig. 1 shows the basic idea and an application scenario of PhoLoc. It is equipped with two sensors: a multi-antenna radio receiver and a low-cost (∼$40) lidar. The radio receiver overhears the cellular signals emitted by a phone to estimate its location at a given moment (e.g., (x_0, y_0) in Fig. 1), while the lidar is to measure the vehicle distance y_s and the time moment t_s when vehicle's front end is firstly detected, which can be used to infer the vehicle length. PhoLoc jointly processes the data from the two sensors to estimate vehicle speed, vehicle length, and phone's *relative* location in vehicle (i.e., Δx and Δy in Fig. 1), and uses the *relative* location to determine if the phone call is being made by the vehicle driver.

The phone localization (estimating phone's location at a given moment) is the core component of PhoLoc. There are three challenges in its design. The **first** one stems from the high mobility of vehicle. For a stationary roadside device, different vehicles may drive at different speeds in a wide range (e.g., from 20 mph to 45 mph). Moreover, PhoLoc does not have prior knowledge of vehicle speed. It must jointly estimate vehicle speed and phone location. The **second** challenge stems from the low packet rate of VoIP data traffic, which is used to support phone calls in 4G LTE and beyond

S. Zhang and H. Zeng are with the Department of Computer Science and Engineering, Michigan State University, East Lansing, MI 48824 USA. The corresponding author is H. Zeng (e-mail: hzeng@msu.edu).

Y.T. Hou is with the Department of Electrical and Computer Engineering, Virginia Tech, Blacksburg, VA 24061 USA.

The work of S. Zhang and H. Zeng was supported in part by NSF Grants CNS-2100112, ECCS-2225337, and CNS-2312448. This work of Y.T. Hou was supported in part by Virginia Commonwealth Cyber Initiative (CCI) and Virginia Tech Institute for Critical Technology and Applied Science (ICTAS).

cellular networks. Per VoIP protocol (G.729 [13]), the VoIP packet rate during a voice call could be as low as 25 packets per second. This agrees with our experimental observations on real-life phone calls. The sparsity of cellular signals makes it difficult to accurately estimate the phone's location at a given time moment. The **third** challenge lies in the fact that vehicle is a scattering-rich environment. Most surely, the radio signals emitted by an in-vehicle phone will go through both light-of-sight (LoS) and non-LoS (NLoS) paths before impinging on PhoLoc's antennas. Since the frame of most vehicles is made of metal materials, the NLoS paths may not be negligible. The presence of non-negligible NLoS paths makes it challenging to accurately localize the phone at a high speed.

While many wireless localization techniques have been developed for mobile devices (e.g., [14], [15], [16], [17], [18], [19]), most of them are based on the estimate of AoA (angle of arrival) or ToF (time of flight) to infer the location of signal source. It is unclear, even if possible, how these techniques can be used to localize a wireless device with high mobility and traffic sparsity in multipath-rich scenarios. To address the above challenges, we propose a new scheme that localizes a moving device using a linear antenna array. Our design was inspired by astronomical interferometer (specifically, VLA in New Mexico [20]). The key idea behind our design is to increase antenna spacing (e.g., 5 ft) so that the antenna array has a large aperture. The large antenna aperture turns a far-field localization problem to a near-field localization problem, making it possible to leverage the movement of vehicle (phone) to generate a concentrated location pattern at a given time moment. Specifically, PhoLoc formulates the localization problem as an optimization problem and searches for the optimal values for the phone's location at a given moment (e.g., (x_0, y_0) in Fig. 1) by maximizing the cross correlation between the measured channels and their projected LoS components over vehicle trajectory.

A critical issue with the proposed near-field localization scheme is channel estimation. In order for PhoLoc (an eavesdropper) to estimate the channel between itself and a phone, it requires fine-grained timing and frequency synchronization between the two devices as well as the knowledge of uplink reference signals from the phone [21]. Moreover, the dynamic resource allocation and user scheduling at cellular base station add another challenge to the channel estimation at PhoLoc. Even if possible, estimating channels will introduce a heavy computational burden on PhoLoc. To address this issue, PhoLoc exploits the signal phase difference over its antennas to localize the target device, which can be extracted from raw baseband signals and therefore eliminates the need of channel estimation. Based on this idea, PhoLoc develops a low-complexity signal processing pipeline for phone localization, which requires neither timing/frequency synchronization nor channel estimation. Since most of prior AoA- and ToF-based localization techniques rely on channel state information (CSI), it is another key difference between our scheme and existing ones.

Based on the new localization scheme, PhoLoc performs system integration and optimization by jointly processing the multimodal data from the two sensors (radio and lidar). It leverages the time duration of vehicle being detected and the average length of personal vehicle to estimate vehicle speed, which may not be accurate but can significantly reduce the time of solving the formulated optimization problem. In addition, PhoLoc analyzes the overheard Bluetooth signals from the vehicle to determine if the driver is making a hand-held or hand-free phone call.

We have built a prototype of PhoLoc using a USRP N310 radio device with 5 ft-separated four antennas and a low-cost lidar sensor. We deployed PhoLoc on a local road's side and drove vehicles at different speeds (from 10 mph to 30 mph) to evaluate its performance. In our experiments, the phone call was made from a vehicle's different seats (driver seat, passenger seat, back-left and back-right seat). Experimental results show that PhoLoc achieves 4.2% false positive rate (FPR) and 13.8% false negative rate (FNR) in the detection of driver's phone call violation.

The contribution of this paper can be summarized as below.

- PhoLoc presents a near-field localization scheme to estimate the location of a moving device at a given time moment. In contrast to prior localization schemes, the proposed scheme does not require channel knowledge for localization.
- PhoLoc combines two distinct sensors, radio and lidar, to localize the *relative* location of a phone inside a vehicle. To the best of our knowledge, it is the first work that estimates the *relative* location of a mobile device at high speed.
- PhoLoc has been evaluated in realistic scenarios. Experimental results confirm the feasibility and effectiveness of PhoLoc in real-life applications.

II. Preliminaries

Most phone carriers in the U.S. (e.g., AT&T, Verizon, and T-Mobile) have officially shut down their 3G networks in 2022 [22]. And after that, 4G and beyond became the dominant cellular networks to provide phone services. In the following, we describe the key features of 4G networks related to PhoLoc. We note that 5G has similar signal structures and protocol stacks as 4G. Therefore, PhoLoc also works with 5G mobile devices.

Uplink Frequency and Bandwidth. Different phone carriers (e.g., AT&T, Verizon, and T-Mobile) have different frequency channels to serve their subscribers. Fortunately, the channel information of each phone carrier is public and available on its website. In the US, the 4G uplink channel frequencies are mainly in the ranges of 650-900 MHz and 1700-2100 MHz [23]. The bandwidth of each channel is 20 MHz, with a sampling rate of 30.72 MSps. While 4G standard supports both TDD and FDD modes [24], most of U.S. cellular networks work in FDD mode.

VoIP for Phone Call. When a phone is on voice call, it will transmit signals to its cellular tower (a.k.a. uplink transmission). Voice-over-Internet-Protocol (VoIP) [25] is used in 4G and beyond networks to carry voice data. G.729 and G.711 are two of the most popular codecs used by VoIP in 4G networks. Per 3GPP [26], mobile VoIP connection sends

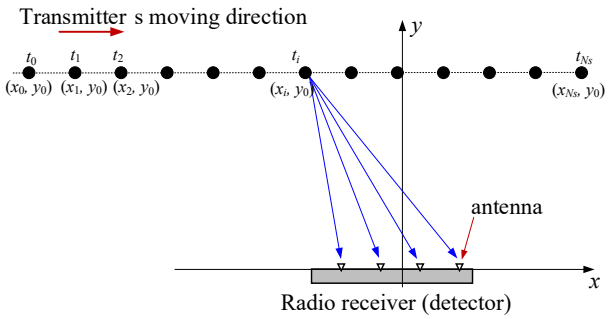

Fig. 2: A problem of localizing a mobile transmitter.

at least 25 VoIP packets per second; and VoIP packet size ranges from 60 bytes to 280 bytes. As will be shown in our experiments, the packet interval from a phone call could be as large as 40 ms. VoIP uses a small bandwidth for RF signal transmission. As it shall be clear, the small bandwidth of VoIP is well suited for PhoLoc's location estimation.

Uplink Signal Transmission. In 4G networks, each user equipment (UE) obtains cell/sector ID and frame timing based on the primary synchronization signal (PSS) and secondary synchronization signal (SSS) that are periodically broadcasted by the base station (BS). UE also uses PSS and SSS to synchronize its carrier frequency with its serving BS. Timing Advance (TA) is used by the BS to inform UE of the time amount that it needs to advance its uplink transmission. The uplink uses single-carrier FDMA (SC-FDMA) [27] modulation scheme for signal transmission. Each UE uses one or more resource blocks (RB, consisting of 12 subcarriers and 7 OFDM symbols) for its data transmission. Demodulation reference signal (DMRS), which is generated based on cell and sector IDs, is included in each RB for channel estimation at BS. Given the complex nature of 4G networks, it is nontrivial for an eavesdropper (PhoLoc) to estimate the channel between itself and a phone.

Uplink Resource Allocation. Cellular networks are a centralized system. BS is the central controller. In uplink, the time and frequency resources are allocated by a BS in a dynamic way [28]. As a result, the frequency of signals emitted by a phone changes over time. As will be shown later, the radio signal emitted by a phone is narrowband in a short time ($\sim$0.1 ms), but its frequency spans over 20 MHz over a long time (about 1 s).

III. Near-Field Localization for Mobile Device

A. Problem Formulation

Consider a mobile single-antenna transmitter and a stationary multi-antenna detector (radio receiver) as shown in Fig. 2.[1] The transmitter is moving at a constant speed v towards the direction in parallel with the detector's linear antenna array, starting from position (x_0, y_0). During its movement, the transmitter sends a packet at time moment t_i, $i = 0, 1, 2, \ldots, N_s$. The detector, at time t_i, receives the data packets and estimates the channel between itself and the transmitter. Denote M as the number of antennas at the detector. Denote $\vec{h}_i = [h_{1i}, h_{2i}, \ldots, h_{Mi}]$ as the measured channel at time t_i. Then, we have

$$h_{mi} = \alpha_{mi0} \cdot e^{-j2\pi \frac{d_{mi0}}{\lambda}} + \sum_{l=1}^{L} \alpha_{mil} \cdot e^{-j2\pi \frac{d_{mil}}{\lambda}}, \quad (1)$$

where α_{mil} is the signal amplitude attenuation for the lth path from the transmitter to the detector's mth antenna at time t_i, d_{mil} is the signal-traveling distance from the transmitter to the detector's mth antenna along the lth path at time t_i. Particularly, $l = 0$ denotes the LoS path. λ is the wavelength of radio signal.

Denote f as the carrier frequency of the transmitter's signal. Denote $(a_m, 0)$ as the coordinate of the detector's mth antenna (see Fig. 2). Then, Equation (1) can be rewritten as:

$$\begin{aligned} h_{mi} = {} & \alpha_{mi0} \cdot e^{-j\frac{2\pi f}{c}\sqrt{(x_0+v(t_i-t_0)-a_m)^2+y_0^2+z^2}} \\ & + \sum_{l=1}^{L} \alpha_{mil} \cdot e^{-j\frac{2\pi f}{c} d_{mil}}, \end{aligned} \quad (2)$$

where c is the radio signal travel speed, z is the elevation (height) difference between the phone and the antennas (not shown in Fig. 2).

In this system, our objective is to estimate the initial location of transmitter (i.e., x_0 and y_0) and its moving speed (i.e., v) based on its observed channel coefficients over time (i.e., $\vec{h}_i$ for $i = 0, 1, 2, \ldots, N_s$). To attain this objective, we exploit the LoS component of channel coefficients for the position estimation. Specifically, we define $\vec{b}_i = [b_{1i}, b_{2i}, \ldots, b_{Mi}]$ as the steering vector at time t_i, with its element being:

$$b_{mi} = e^{-j\frac{2\pi f}{c}\sqrt{(\hat{x}_0+\hat{v}(t_i-t_0)-a_m)^2+\hat{y}_0^2+\hat{z}^2}}. \quad (3)$$

Then, the localization problem can be formulated as follows:

$$[\hat{x}_0^*, \hat{y}_0^*, \hat{v}^*] = \arg\max_{\hat{x}_0, \hat{y}_0, \hat{v}, \hat{z}} \sum_{i=0}^{N_s} \left| \vec{h}_i \vec{b}_i^{\mathsf{H}} \right|, \quad (4)$$

where $(\cdot)^{\mathsf{H}}$ is conjugate transpose operator.

We note that the observed channels at a detector include not only over-the-air response but also RF circuitry response. While the LoS component of over-the-air channel phase can be inferred based on phone's location, the radio frequency (RF) circuitry response may randomly vary over packet transmissions. To eliminate this uncertainty, we exploit the relative channel phases over antennas for the problem formulation. That is the reason why the `abs` operation is used in Equation (4).

B. Antenna Spacing

For a given number of antennas at the detector, the solvability of Equation (4) is determined by its antenna spacing. In most prior works on both wireless localization and communications, the antenna spacing is assumed to be less than wavelength (e.g., half wavelength). With such a small antenna spacing, the transmitter is considered to be in the far field of the detector. The antenna aperture of the detector is

[1]For ease of exposition, we assume that the transmitter has a single antenna. In general, our approach works for the case where the transmitter has multiple antennas.

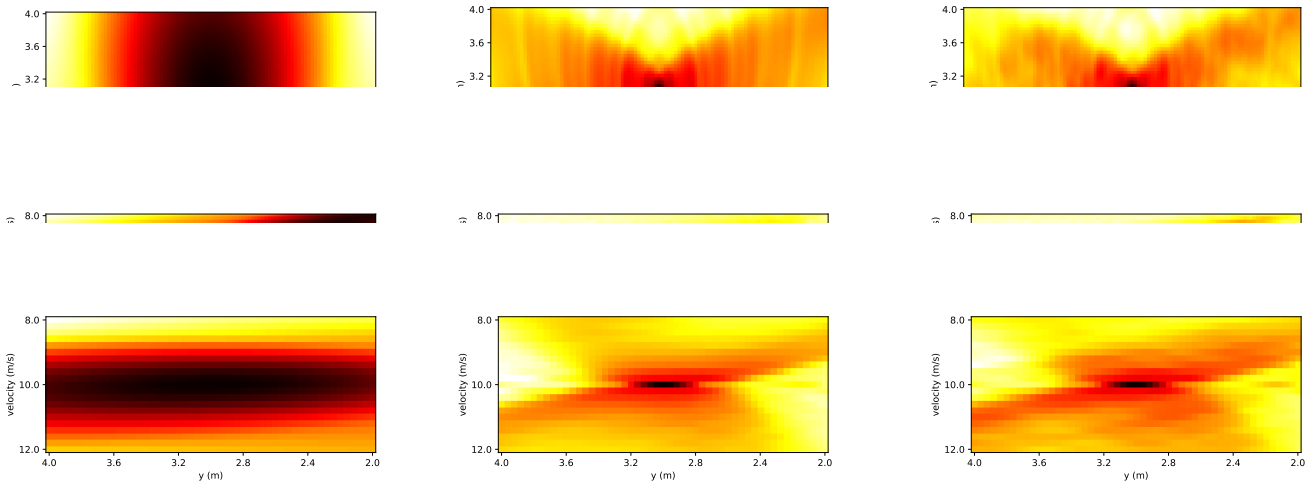

(a) $\lambda/2$ antenna spacing in a LoS scenario. (b) 1.5 m antenna spacing in a LoS scenario. (c) 1.5 m antenna spacing in LoS+NLoS scenario.

Fig. 3: Localizing mobile device in far-field and near-field scenarios. In each subfigure, a large black area means that the localization is not feasible. A small black area (dot) means that the vehicle can be accurately localized.

small and, as a result, the angular resolution of the detector is very limited. In such a case, the problem in Equation (4) easily becomes unsolvable. This is because the LoS-path phase difference over antennas lacks dynamic range, making it impossible to infer the starting location of transmitter based on channel observations.

To show the relationship between the antenna spacing and the solvability of Equation (4), let us consider the case in Fig. 2 for example. Assume that the carrier frequency is $f = 1890$ MHz. The starting location of the transmitter (phone) is $(x_0, y_0) = (-10.0,\ 3.0)$. The speed is $v = 10.0$ m/s. The detector and transmitter are on the same height (i.e., $z = 0$ and $\hat{z} = 0$). The number of antennas at the detector is $M = 4$. The antenna spacing is half wavelength ($\lambda/2$). Let us further assume that there exists only LoS path between transmitter and detector (i.e., no NLoS path between them). In such a setting, we simulate the channels from the M antennas (i.e., $\vec{h}_i$ for $i = 1, 2, \ldots, N_s$) and then solve Equation (4) to find the initial location of the transmitter. Fig. 3a shows the results of exhaustive search for the optimal solution to Equation (4). Evidently, when the antenna spacing is small, it is hard to find the optimal solution to Equation (4).

To make the problem solvable, we transform the far-field localization problem to a near-field localization problem by increasing the detector's antenna spacing. Specifically, we set the antenna spacing to 1.5 m. Fig. 3b shows the results of exhaustive search for the optimal solution to Equation (4). It is clear to see that the optimal solution can be found, and the corresponding values of $\hat{x}_0^*$, $\hat{y}_0^*$, and $\hat{v}^*$ can be accurately estimated. In the above cases, we assumed that the channel has only LoS path (i.e., no NLoS path). A natural question to ask is whether the problem is solvable when the channel has non-negligible NLoS paths. To explore the answer to this question, we consider a case where there are both LoS and NLoS paths between transmitter and detector. The strength of LoS path is 1; and the strength of three NLoS paths are $[0.5, 0.25, 0.125]$. The three NLoS paths are caused by three objects around the transmitter, with coordinate offsets $(2, 0)$, $(0, 1)$, and $(1, 2)$. Fig. 3c shows the numerical results. It can be seen that the optimal values of $\hat{x}_0^*$, $\hat{y}_0^*$, and $\hat{v}^*$ can still be clearly identified. This can be attributed to the fact that LoS and NLoS paths are typically uncorrelated over time.

C. Impact of Antenna Height

The problem in Equation (4) involves four optimization variables ($\hat{x}_0$, $\hat{y}_0$, $\hat{v}$, and $\hat{z}$), leading to a computational challenge in finding their optimal variables. For PhoLoc, the antenna height information is not needed for determining the relative location of phone in a vehicle. Hence, we study the impact of antenna height z on the estimation of other variables (i.e., x_0 and y_0). If the estimation of those variables is not sensitive to z, we can replace it with an estimated value in Equation (4). Doing so will reduce the optimization search space from four to three dimensions, thereby reducing the required computation. For personal vehicles, the average height of a sedan car is about 1.4 m, the average height of an SUV is about 1.9 m, and the average height of a pick-up is about 1.9 m. If we fix the antenna height of PhoLoc to 1.65 m, then the height error in Equation (4) should be less than 0.5 m for most cases. We therefore use 0.5 m as the upper bound of antenna height error to study its impact on the correlation value and the estimates of other parameters.

Consider the detector with four antennas as shown in Fig. 2, with the same parameters listed in §III-B. The detector has four linear antennas with a spacing of 1.5 m. In this case, we study the impact of antenna height error (error of z) on the estimates of (x_0, y_0, v), as well as its impact on the correlation result. Fig. 4 presents our numerical results. It is evident that the search of x_0, y_0, and v is not sensitive to the antenna height error in both LoS and NLoS scenarios. The antenna height error has a negligible impact on the estimates of x_0 and v. It has a slight impact on the estimate of y. A 0.5 m error of z will introduce 0.04 m error of y, which is tolerable in practice.

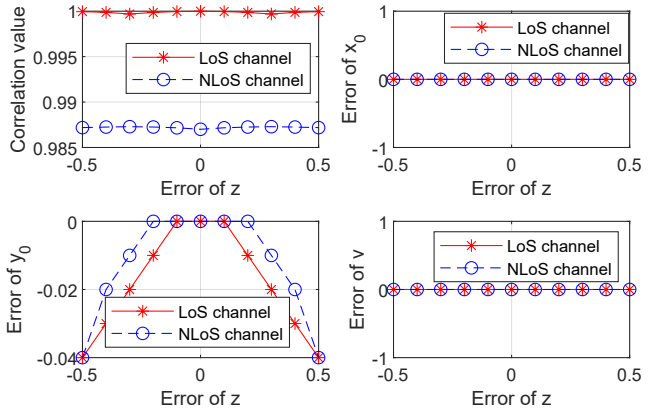

Fig. 4: Impact of elevation error on the estimates of other parameters. Top-left: impact on correlation value; top-right: impact on the estimate of x_0; bottom-left: impact on the estimate of y_0; bottom-right: impact on the estimate of v.

To see the reason why the estimates of (x_0, y_0, v) are resilient to the error of z, let us focus on the `sqrt` term in Equation (3). In practice, since $(\hat{x}_0+\hat{v}(t_i-t_0)-a_m)^2+\hat{y}_0^2 \gg \hat{z}^2$, the removal of $\hat{z}$ will generate a negligible impact on the final results, as demonstrated in Fig. 4. Therefore, we redefine the element of steering vector $\vec{b}_i = [b_{1i}, b_{2i}, \ldots, b_{Mi}]$ as follows:

$$b_{mi} = e^{-j\frac{2\pi f}{c}\sqrt{(\hat{x}_0+\hat{v}(t_i-t_0)-a_m)^2+\hat{y}_0^2}}. \quad (5)$$

The removal of $\hat{z}$ will significantly reduce the optimization space to find the optimal values of (x_0, y_0, v), thereby reducing the computation of PhoLoc.

D. Impact of Speed Change

Our model to find the location of a mobile device is based on the assumption that the driving speed of the vehicle is constant. To fulfill this assumption, PhoLoc should not be installed at the locations close to intersections or STOP sign. Rather, it should be installed at road segments where vehicles drive straightly and smoothly. As a roadside detection device designed to assist traffic management authorities in implementing safety policies, being placed in these locations is not an extravagant request. In this part, we study the impact of vehicle speed change on the estimate of its location. We consider two most common cases: vehicle acceleration and vehicle braking. To minimize the impact of various speeds, we do not estimate the starting location of phone. Instead, we estimate the middle location of phone when its trajectory intersects with y axis (see Fig. 2).[2]

Since it is hard to analytically characterize the impact of speed change, we resort to the numerical method again. We consider the scenario described in §III-B. The detector collects radio signals from the transmitter (phone in vehicle) when $x \in [-15, 15]$. The moving distance of vehicle is modeled as $d = vt+\frac{1}{2}at^2$, where $v \in \{10, 20, 30\}$ and a is the acceleration rate of vehicle ranging from -2 m/s^2 to 2 m/s^2. Fig. 5 depicts

[2]As we will show in the next section, the middle location (not the starting location x_0) will be adopted in our design to minimize the cumulative errors from various sources.

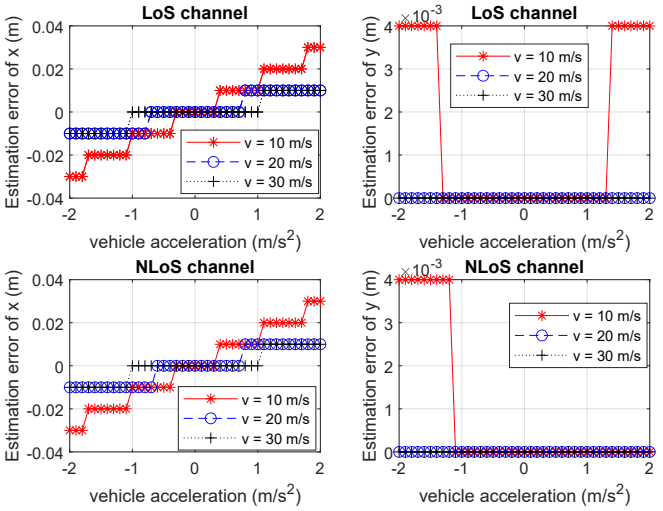

Fig. 5: Impacts of vehicle acceleration on the estimates of x and y in two scenarios: LoS channel and NLoS channel.

the estimation error of x (the estimated horizontal coordinate of phone) and y (the estimated vertical coordinate of phone) in LoS and NLoS scenarios. The discrete estimation errors in the figure stem from the fixed search steps, i.e., 0.01 m for x and 0.001 m for y. It can be seen that the estimation error of x is less than 0.04 m for both LoS and NLoS scenarios. It can also be seen that the estimation error of y is less than 0.005 m for both scenarios. The numerical results, albeit from a single case study, indicate that the proposed approach is resilient to vehicle acceleration and braking.

In practice, PhoLoc collects cellular signal from phone for localization only when it is within its proximity. The time duration of signal collection is typically less than 2 seconds. During such a short time, there are many road segments where vehicles drive straightly and smoothly with speed change less than 2 m/s^2. However, a vehicle may not simply be accelerating or braking. The speed change is still a main source of estimation error for PhoLoc.

IV. Design

A. Basic Idea

PhoLoc aims to determine if the driver of a vehicle is on a phone call. To do so, it needs to know the relative location of a phone in a vehicle rather than its absolute location. To find out the phone's relative location, PhoLoc is equipped with two sensors: i) a lidar sensor, and ii) a multi-antenna radio receiver. The lidar sensor serves for two main purposes. *First*, it records the time moment when the vehicle is initially detected (i.e., the vehicle's front end being detected). We denote this time moment as t_s, which will be used to calculate the relative horizontal location of the phone. *Second*, it measures the distance between itself and the one side (either left or right side) of vehicle. We denote the measured distance as y_s, which will be used to infer the relative vertical location of phone. An illustration of y_s can be found in Fig. 1.

The multi-antenna radio receiver will be used to *overhear* cellular radio signals emitted by the phone. We increase its

antenna spacing (5 ft in our experiments) to turn the far-field localization problem to a near-field localization problem. Then, based on the overheard cellular signal, it estimates (x_0, y_0, v) by solving the problem in Equation (4). Combining the measurement results from the two sensors, the relative location of the phone within a vehicle, which we denote as $(\Delta x, \Delta y)$, can be calculated as follows:

$$\Delta x = (t_s - t_0)v - x_0, \tag{6a}$$

$$\Delta y = (y_0 - y_s), \tag{6b}$$

where x_0, y_0, v, and t_0 are obtained from the multi-antenna radio detector, while t_s and y_s are obtained from the lidar sensor.

B. Phone Localization Without CSI

Challenges and Approaches. Solving the problem in Equation (4) to obtain (x_0, y_0, v) requires the channel knowledge $\vec{h}_i$ at time t_i, $i = 0, 1, 2, \cdots$. However, since PhoLoc acts as an eavesdropper and does not perform direct communication with the phone, it is challenging for PhoLoc to estimate the channel coefficients between the phone and itself. This is because estimating the channel coefficients requires the knowledge of demodulation reference signals embedded in the phone's signal frames. It also needs to compensate the timing and frequency offsets of each signal frame. These requirements pose a grand challenge in the design of PhoLoc. Even if possible, estimating channel coefficients will impose an intimidating computational requirement on the implementation of PhoLoc. It is worth noting that, for PhoLoc, synchronizing itself with a phone is much more difficult than synchronizing itself with a base station. This is because a base station periodically broadcasts PSS and SSS, but a phone does not broadcast such signals for synchronization.

To address this challenge, we revisit the problem formulation in Equation (4) with the aim of eliminating the need of channel knowledge. Based on Equation (2) and Equation (3), it can be seen that the correlation (inner product) in Equation (4) is to exploit the signal phase difference over different antenna elements. Fortunately, the signal phase difference over antennas can be estimated based on the received baseband signal, requiring neither timing/frequency synchronization nor channel estimation. Inspired by this observation, we will propose a practical scheme to estimate the signal phase difference over largely-separated antenna elements.

To estimate the relative signal phases at PhoLoc, there is another challenge that stems from the time-varying frequency of phone signal. A base station and its serving phones are working in master-slave mode. The base station dynamically allocates one or more resource blocks (12 OFDM subcarriers $\times$ 7 OFDM symbols) for the uplink transmission of its serving phones so as to improve the spectral efficiency. The allocated resource blocks for a phone change rapidly over time. Fig. 6 shows an example of a real-life T-Mobile phone's signal frequency when making a voice call. It can be seen that the signal frequency is not fixed but changes rapidly. To address this challenge, the time-varying signal frequency needs to be taken into account in the problem formulation; and its impact should be eliminated.

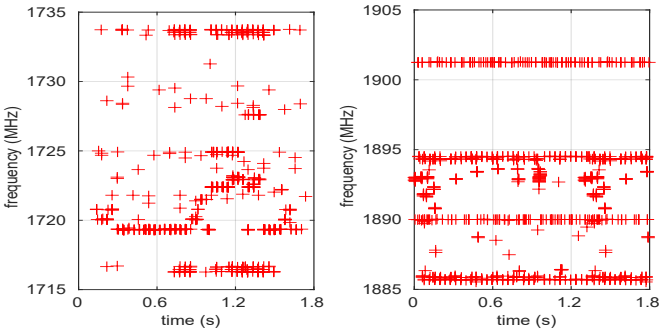

Fig. 6: An example of phone signal's frequency and timestamp. The phone uses T-mobile networks, and it works on two frequency bands: 1720 MHz and 1890 MHz.

Phone Localization. Based on the results in §III, we propose a phone localization scheme that requires neither timing/frequency synchronization nor channel estimation, while accounting for the time-varying frequency of phone signals. Fig. 7 depicts the diagram of our proposed phone location scheme, which consists of the following three components.

• *Phone signal search.* When a vehicle is approaching, PhoLoc first needs to figure out two questions: i) is there an active phone call in the vehicle? and ii) what is the uplink frequency channel used by the phone call? To find the answers to these two questions, PhoLoc monitors the power level and spectrum pattern of radio signals over all possible uplink cellular channels (e.g., 1.5 GHz – 3.6 GHz). If cellular signals are periodically detected above a predefined power threshold, then it believes there is an active phone call in the vehicle and its frequency channel can be identified accordingly. This approach is effective in practice due to two facts. **First**, in our problem setting, the vehicle of interest is very close to PhoLoc (e.g., 10s meters). Hence, PhoLoc will consistently observe distinctly strong phone signals if there is an active phone in the vehicle. In addition, since the vehicle is driving toward PhoLoc, the observed phone signal power at PhoLoc is continuously increasing. These features make it easy for PhoLoc to detect active phone calls in vehicles and their associated frequency channels. **Second**, thanks to the advances in software-defined radio (SDR) technologies, the spectrum monitoring of multiple channels can be achieved in a rapid manner. As PhoLoc only needs a small amount of phone signal data for localization (e.g., less than 2 seconds for signal collection in our experiments), there is ample time for PhoLoc to monitor the spectrum of all uplink cellular channels when a vehicle is driving toward PhoLoc. This feature makes it possible for PhoLoc to localize multiple phones on different frequency bands inside a vehicle.

• *FFT.* This module converts the phone signal from the time domain to the frequency domain. PhoLoc uses 30.72 MHz sampling rate and 2048 FFT points for this module. We emphasize that PhoLoc does not have timing/frequency estimation and compensation before the FFT operations.

• *Phone signal extraction.* A phone may use one or more resource blocks for its data transmission when making a

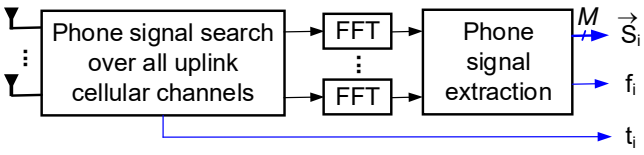

Fig. 7: The schematic diagram of our signal acquisition scheme for PhoLoc.

voice call. When a phone uses multiple resource blocks for transmission, its wideband signal obscures the phase difference over PhoLoc's antennas. Hence, we select a subset of strong adjacent subcarriers for signal phase difference estimation. Denote y_{mik} as the FFT results, where m is antenna index, i is data sample index, and k is subcarrier index. Denote $\mathcal{R}_i$ as the subset of subcarriers selected for phase estimation. Then, we let

$$\mathcal{R}_i = \big\{k : |k - k_{\max}| < N_{RB}/2, |y_{mik}| > \eta y_{\max}\big\}, \quad (7)$$

where N_{RB} is the number of subcarriers in a resource block ($N_{RB} = 12$ in 4G LTE); $k_{\max}$ and $y_{\max}$ are the index and amplitude of the strongest subcarrier, respectively; η is an empirically-selected threshold ($\eta = 0.3$ in our experiments).

After selecting the subset of subcarriers, we construct the signal vector as follows:

$$\vec{s}_i = [s_{1i}, s_{2i}, \cdots, s_{Mi}], \quad (8)$$

where $s_{mi} = \frac{\sum_{k\in\mathcal{R}_i} y_{mik}}{|\sum_{k\in\mathcal{R}_i} y_{mik}|}$. The rationale behind the normalization operation is that the signal phase carries the information of interest while the signal amplitude does not.

The corresponding frequency of $\vec{s}_i$ can be approximately written as:

$$f_i = f_c + \frac{\sum_{k\in\mathcal{R}_i} k}{|\mathcal{R}_i|}\frac{f_s}{N_{\text{fft}}}, \quad (9)$$

where $|\cdot|$ is the cardinality of a set, f_c is the center frequency, f_s is signal sampling rate, and N_{fft} is FFT size. In PhoLoc, $f_s = 30.72$ MHz and $N_{\text{fft}} = 2048$.

With signal vector $\vec{s}_i$, its frequency f_i, and its timestamp t_i, we reformulate the localization problem in Equation (4) as follows:

$$[\hat{x}_0^*, \hat{y}_0^*, \hat{v}^*] = \arg\max_{\hat{x}_0,\hat{y}_0,\hat{v}} \sum_{i=0}^{N_s} \left|\vec{s}_i \vec{b}_i^{\mathsf{H}}\right|, \quad (10)$$

where the element of steering vector $\vec{b}_i = [b_{1i}, b_{2i}, \cdots, b_{Mi}]$ is rewritten as:

$$b_{mi} = e^{-j\frac{2\pi f_i}{c}\sqrt{(\hat{x}_0+\hat{v}(t_i-t_0)-a_m)^2+\hat{y}_0^2}}. \quad (11)$$

For the operations in Fig. 7, we have the following two remarks.

Remarks. We have two remarks for the above signal acquisition for phone localization. First, without frequency and timing offset compensation before FFT, the estimated frequency-domain symbols (the output of FFT in Fig. 7) will not follow the classic wireless communication model of $y = hx+n$, where y is received signal, h is channel coefficient, and x is the transmission signal. Neither can they represent the real channels. Nevertheless, the phase difference of frequency-domain signals ($\vec{s}_i$) is an approximation of their channels' phase difference. Second, as shown in Fig. 7, PhoLoc is different from a typical multi-antenna receiver. It does not have frame detection, frequency/timing estimation and compensation, and channel estimation. Removal of these signal processing blocks significantly simplifies the implementation of PhoLoc.

C. Joint Optimization for Lidar and Radio Receiver

Using Equation (6) to estimate $(\Delta x, \Delta y)$ faces two challenges. First, radio receiver and lidar sensor have very different data sample rates. Per 3GPP, the VoIP packet interval is up to 40 ms, yielding a data sample rate of 25 Hz. If lidar measures the distance at VoIP packet rate, the measurement error could be as large as 1 m when vehicle is driving at 25 m/s. Therefore, the measurement data from radio receiver and lidar sensor should be synchronized for phone localization. Second, per Equation (6a), if v is not a constant, a cumulative error will be generated for the estimate of Δx. To minimize the cumulative error, we use the near-field localization algorithm to estimate the phone location at time t_s instead of time t_0. Doing so will not only resolve the low packet rate issue but also reduce the cumulative error from the inaccurate speed estimation.

Mathematically, we define (x_p, y_p) as the phone's coordinate at the moment t_s (i.e., the vehicle's front end is just detected by lidar). Per Equation (6), we have $\Delta x = -x_p$ and $\Delta y = y_p - y_s$. Then, based on Equation (11), we rewrite the elements of steering vector $\vec{b}_i = [b_{1i}, b_{2i}, \cdots, b_{Mi}]$ as follows:

$$b_{mi} = e^{-j\frac{2\pi f_i}{c}\sqrt{(-\Delta\hat{x}+\hat{v}(t_i-t_s)-a_m)^2+(\Delta\hat{y}+y_s)^2}}, \quad (12)$$

where Δx, Δy, and y_s are illustrated in Fig. 1.

Finally, the phone localization problem can be expressed as:

$$[\Delta\hat{x}^*, \Delta\hat{y}^*, \hat{v}^*] = \arg\max_{\Delta\hat{x},\Delta\hat{y},\hat{v}} \sum_i \left|\vec{s}_i \vec{b}_i^{\mathsf{H}}\right|, \quad (13)$$

where $\vec{s}_i$ is given in Equation (8) and $\vec{b}_i$ is given in Equation (12).

To solve Equation (13), there are three variables that need to be searched. For most personal vehicles (Sedan and SUV), their length is less than 5 m and their width is less than 2 m. Therefore, we empirically set the search range of $\Delta\hat{x}$ to $[0, 5]$ and the search range of $\Delta\hat{y}$ to $[-0.5, 2.5]$. A question to ask is what is the range of $\hat{v}$. In practice, the speed of vehicles may be very different at the same location (e.g., from 20 mph to 45 mph). To reduce the search space, we leverage the data from lidar. Denote τ as the time duration of vehicle passing the lidar. Since the average length of personal vehicles is 4.6 m, we set a reference speed as $v_{ref} = 4.6/\tau$. Then, we empirically set the search range of $\hat{v}$ to $[0.7v_{ref},\ 1.3v_{ref}]$. As the search problem in Equation (13) is naturally suitable for parallel computing, we use exhaustive search to pursue its optimal solution in our experiments. By using 8 threads on an i7-10700 CPU, it takes less than 2 seconds to find the optimal solution in our experiments.

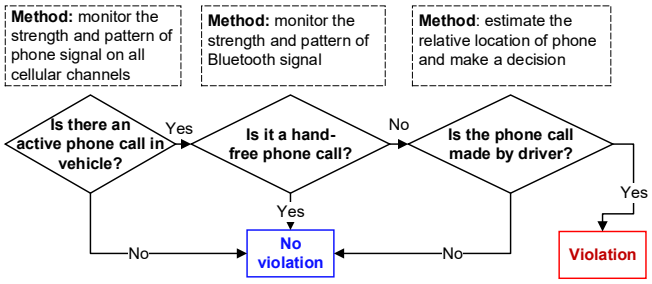

Fig. 8: PhoLoc's decision tree of detecting the violation of phone call.

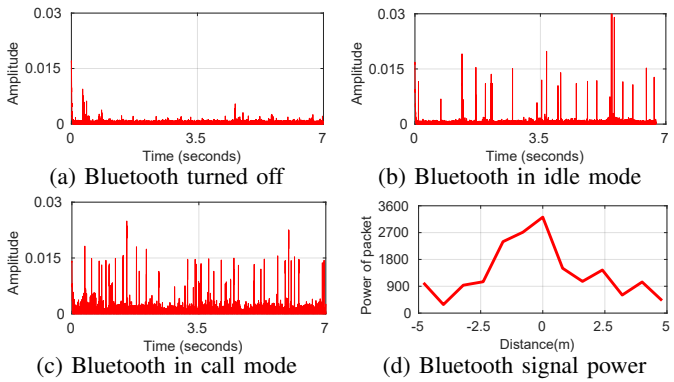

(a) Bluetooth turned off (b) Bluetooth in idle mode (c) Bluetooth in call mode (d) Bluetooth signal power

Fig. 9: Bluetooth traffic intensity and relative signal power in different modes.

Denote c^* as the optimal normalized correlation value. Then, it can be written as:

$$c^* = \frac{1}{M(N_s+1)} \left[\sum_{i=0}^{N_s} \left| \vec{s}_i \vec{b}_i^{\mathsf{H}} \right| \right]_{\Delta\hat{x}=\Delta\hat{x}^*, \Delta\hat{y}=\Delta\hat{y}^*, \hat{v}=\hat{v}^*}, \quad (14)$$

where M is the number of antennas and N_s+1 is the number of data samples.

D. Put it All Together

Fig. 8 depicts the overall diagram of PhoLoc to detect the violation of driver's phone call. Some steps are described as follows.

Bluetooth Hand-Free Detection. Bluetooth-based hand-free phone call while driving is permitted in some countries and areas. Fortunately, hand-free phone calls can be easily detected by the roadside infrastructure, thanks to the different frequency bands of cellular and Bluetooth signals. Fig. 9 shows the Bluetooth signals collected by a roadside radio receiver (5 m distance) from a Toyota vehicle. It can be seen that the traffic intensity is significantly different when vehicle Bluetooth is in different modes. It can also be seen that the Bluetooth power decays rapidly over distance. These observations indicate that the use of Bluetooth for hand-free phone call can be reliably detected through monitoring Bluetooth's traffic intensity and frequency.

Decision Making. After computing the optimal values for Equation (13) and Equation (14), PhoLoc detects the violation of driver's phone call as follows:

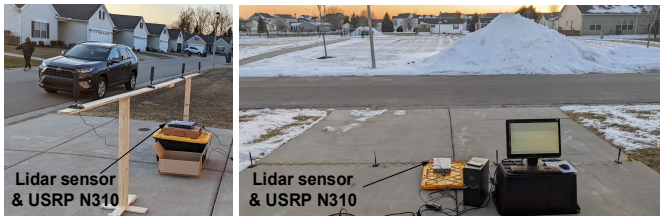

Fig. 10: Photos of PhoLoc with lifted antennas (left) and on-ground antennas (right).

$$\mathcal{D} = \begin{cases} \text{violation of phone call} & \text{if } \Delta x^* \geq x_{\text{th}},\ \Delta y^* \leq y_{\text{th}},\ c^* \geq c_{\text{th}}, \\ \text{no violation} & \text{otherwise,} \end{cases} \quad (15)$$

where x_{th}, y_{th}, and c_{th} are the thresholds used to make the decision. Threshold c_{th} can be used to balance the false positive and negative rates of PhoLoc. In our experiments, we empirically set $c_{\text{th}} = 0.61$. For x_{th} and y_{th}, PhoLoc does not simply set them to fixed values. Instead, it first estimates the vehicle length by $L_{veh} = \hat{v}^*\tau$, where τ is the time duration of vehicle being detected by lidar sensor. Based on the vehicle length, PhoLoc empirically sets their values as follows: $(x_{\text{th}}, y_{\text{th}}) = (2.70, 0.93)$ if $L_{veh} \leq 4.9$ m and $(x_{\text{th}}, y_{\text{th}}) = (2.80, 0.96)$ otherwise. Note that PhoLoc targets the detection for personal vehicles only (e.g., sedan and SUV). More sophisticated methods can be exploited to set values for those three thresholds.

V. Experimental Evaluation

A. Implementation

Fig. 10 shows our prototype of PhoLoc, which was built using a USRP N310, a lidar, a PC, and four LTE antennas.

Radio Device. We have built a prototype of PhoLoc's radio receiver using USRP N310 device, which has 4 channels with frequency ranging from 10 MHz to 6 GHz and supports 100 MHz instantaneous bandwidth. The USRP device is connected with a Dell XPS desktop (i7-10700 CPU, 16 G RAM) via 10 Gigabit SFP+ Ethernet. Four low-cost LTE antennas with 8 ft cables are installed on USRP N310 for cellular signal reception.

Lidar Sensor. We use MakerFocus TFmini-s module ($43 on Amazon [29]) as PhoLoc's lidar sensor to measure the distance between itself and a vehicle. Per its manual, this module offers a 0.1 m–12 m measurement range with 1000 Hz measurement frequency. Its distance resolution is 1 cm, and its ranging accuracy is 6 cm or 1% of its measurement distance. Our lab tests show that the max measurement frequency is 876 Hz. The lidar sensor is connected with the same Dell computer via USB interface, and their communication protocol is UART.

Software. We implement the software of PhoLoc using GNU Radio Out-of-Tree (OOT) module [30]. The signal processing blocks in Fig. 7 was implemented in C++. Each block in Fig. 7 was implemented in a separate thread for parallel computing to realize real-time computation. The distance data acquired from the lidar sensor is sent to GNU Radio [31] for

Fig. 11: Phone caller is on different seats.

data fusion. All radio and lidar data samples are timestamped using the radio sampling rate (30.72 MHz).

Experimental Setup. As shown in Fig. 10, two antenna configurations are considered in our experiments: i) antennas are fixed at 3.5 ft height, and ii) antennas are placed on the ground. Three persons (two drivers and one passenger) were involved in our experiments. The driver or a passenger held a T-Mobile phone for voice calls (via VoLTE) by placing the phone at three different spots: left ear, right ear, and in front of the mouth, as shown in Fig. 11. Another T-Mobile phone was also placed inside the vehicle to play online music. It served as a potential interference source, generating bursty data traffic other than VoIP traffic. We note that we did not intentionally turn off other data traffic generated by these two phones from their other apps. During the tests, vehicle windows remain closed. Throughout our experiments, we used two vehicles for testing: Toyota RAV4 and Toyota Camry. PhoLoc does not have prior knowledge of vehicles when detecting the violation of phone calls.

B. In-Lab Validation

Before we conduct on-road tests, we first validate the proposed near-field localization scheme in lab. We place PhoLoc and a phone on a laboratory floor. PhoLoc has four antennas and the antenna spacing is 1 m. The antenna coordinates are (-1.5, 0), (-0.5, 0), (0.5, 0), and (1.5, 0). We move a T-Mobile phone, which is on an active voice call, from (-2.5, 0) to (2.5,0) with a step size of 5 cm, as illustrated in Fig. 12. A total of 101 data samples are collected. Based on the collected data, we use the formulation in Equation (10) to search for the starting position of the phone (i.e., x_0 and y_0).

Fig. 13 shows the inverse heatmap of search results. The estimated start location is (-2.520, 0.995). This means that the estimated error of x_0 is 2 cm and the estimated error of y_0 is 0.5 cm. Fig. 13 also shows the normalized coordination along the x and y axes. It can be seen that the correlation peak is evident along both x and y axes. The results reveal the robustness of the proposed near-field localization scheme.

C. A Case Study on Road

We deployed PhoLoc on the roadside as shown in Fig. 10. The four antennas were lifted to 3.5 ft (1.07 m), and the antenna spacing was 5 ft (1.524 m). The lidar sensor was

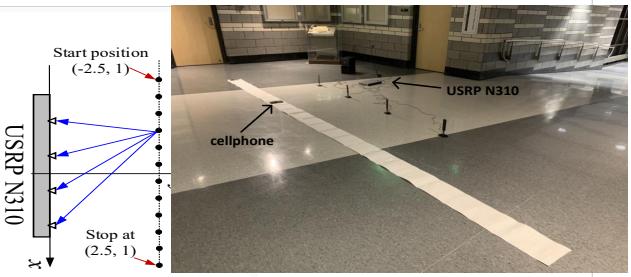

(a) Setup. (b) A photo of experimental setup.

Fig. 12: Experimental setup for in-lab validation.

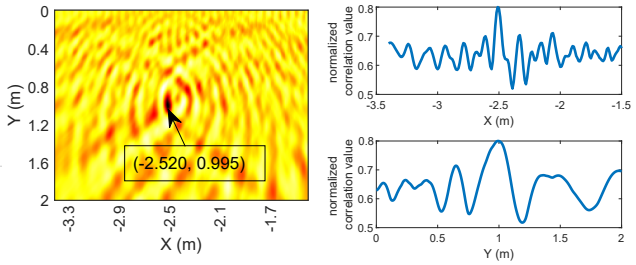

Fig. 13: Experimental results of finding the starting location of phone. [Left]: Inverse correlation heatmap generated by PhoLoc. [Right]: Normalized correlation along the x and y axes.

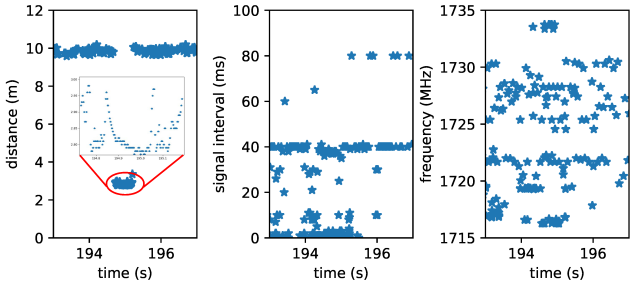

Fig. 14: Lidar's distance output (left), signal sample interval (middle), signal frequency (right).

placed in the exact middle of four antennas, facing to the road. A person drove a vehicle (Toyota RAV4) on the road from the right to the left. The driver was on a phone call, and his cellphone used T-Mobile 4G service. He held his cellphone on his left ear, without Bluetooth for a hand-free connection. The vehicle's speedometer reads 20 mph.

Lidar Measurement. Fig. 14 (left) shows the lidar's data. PhoLoc reads the lidar's measurement once per millisecond. The lidar sensor detected the vehicle for a duration of $\tau = 0.47$ s. Hence, the vehicle's speed is estimated to $4.6/0.47 = 9.78$ m/s, where 4.6 is the average length of all personal vehicles on market. Based on the estimated speed, we set the search range of $\hat{v}$ to $[0.70 \times 9.78, 1.3 \times 9.78]$, with a step size of 0.02 m/s. The optimal value turns out to be 9.47 m/s, which is very close to the estimated value. Then, let us zoom in the distance measured by lidar on Fig. 14 (left). It can be seen that the measured distance varies from 2.8 m to 3.0 m. To reduce the measurement error, we exclude the measurements on the two sides and take average of the remaining measurements. The result is used as y_s, which is 2.86 m for this case.

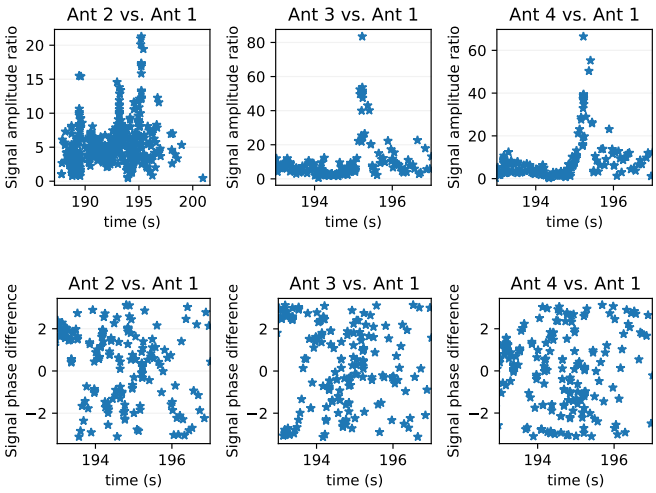

(b) Signal phase difference of four antennas.

Fig. 15: Collected signal samples from radio receiver.

Signal Interval and Frequency. Fig. 14 (middle) shows the signal intervals of phone's transmissions measured by PhoLoc. It can be seen that, for most of time, the signal time interval is 40 ms. This is consistent with the VoIP standard. For this case, signal samples of 1.49 s time duration were used by PhoLoc to estimate the phone location, corresponding to 14 m moving distance of the vehicle. The right figure in Fig. 14 plots the frequency of phone signals. It is centered around 1725 MHz, spanning over 20 MHz. It can be seen that the transmission frequency of phone's packets changes rapidly over time. This is because the transmission frequency of a phone is dynamically scheduled by its associated base station.

Signal Amplitude and Phase. Fig. 15a shows the signal amplitude ratio of the receiver's four antennas. Fig. 15b shows their phase difference. It can be seen that the signal amplitudes are very dynamic. We normalize the signal amplitudes so the phase of each signal sample carries the same weights. While the phase looks noisy, it actually bears some patterns caused by the movement of vehicle. The inherent pattern plays a key role in the inference of phone location.

Correlation Heatmap. Based on the collected data from radio and lidar, PhoLoc did a brutal-force search to find the optimal solution to Equation (13). The resultant optimal values are $\Delta\hat{x}^* = 2.09$ m, $\Delta\hat{y}^* = 0.46$ m, $\hat{v}^* = 9.48$ m/s, and $c^* = 0.7$. Fig. 16a shows the generated inverse heatmap of correlation from PhoLoc, where dark pixels represent high correlation while light pixels represent low correlation. The inverse heatmap clearly manifests its peak, which is concentrated in a small area.

Decision and Estimation Errors. Based on the optimized vehicle speed, the vehicle length is estimated to be $L_{veh} = \hat{v}^*\tau = 9.48 \times 0.47 = 4.45$ m, where τ is the time duration of vehicle being detected by lidar. Since $L_{veh} \leq 4.9$, we let $(x_b, y_b) = (2.7, 0.93)$ based on our predefined criteria. Then, per Equation (15), the phone location in this case will be classified to driver seat. Our manual measurements show that $\Delta x = 2.25$ m and $\Delta y = 0.36$ m. While they are not very accurate, we use them as the ground truth. Then, the errors of PhoLoc is $\mathcal{E}_x = 16$ cm and $\mathcal{E}_y = 10$ cm in this case.

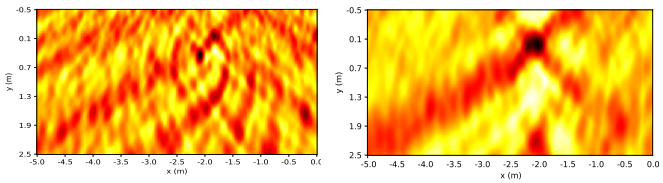

(a) 3.5 ft antenna height. (b) On-ground antennas.

Fig. 16: Inverse correlation heatmap generated by PhoLoc when its antennas are of different heights.

Impact of Antenna Height. Previously we showed that PhoLoc is not sensitive to antenna height via simulation. We now test this hypothesis using experiments. We repeated the above case study but placing antennas on ground as shown in Fig. 10. This setup brings about 1.5 m error for antenna height z in the search of phone's location. Fig. 16b shows the heatmap generated by PhoLoc. Comparing the two figures in Fig. 16, it can be seen that the large error of antenna height does degrade PhoLoc's performance. Therefore, in the rest of our experiments, we use the experimental setup where the four antennas are fixed to 3.5 ft height.

D. Impact of Antenna Spacing

We repeated the experiment described in the above case study when PhoLoc has different antenna spacings: 2 ft, 3 ft, 4 ft, and 5 ft. For each case, we conducted 15 tests. The driver is the same, and the vehicle is the same. The driver placed his phone on his left ear. The vehicle speed is around 20 mph. Fig. 17 shows inverse heatmap examples when PhoLoc has different antenna spacings. Fig. 18 shows the measurement results for the first five tests in each case. It is evident that PhoLoc performs poorly when the antenna spacing is small. Increasing the antenna spacing tends to improve the performance of PhoLoc. Of the 15 tests, the standard deviation of $(\Delta x, \Delta y)$ is (0.11, 0.72) in the 2 ft spacing case, (0.10, 0.16) in the 3 ft spacing case, (0.12, 0.10) in the 4 ft spacing case, and (0.06, 0.08) in the 5 ft spacing case.

A question to ask is if a larger antenna spacing is always better. Our observation is no. A larger antenna spacing requires a vehicle to maintain a constant speed in a longer distance. In addition, the vehicle's trajectory should be in stricter parallel with antenna array. That means that PhoLoc with a larger antenna spacing is more sensitive to vehicle's speed change and direction error. In addition, it will require more spacing for deployment. Based on the above considerations, we recommend that PhoLoc use 5 ft as its antenna spacing.

E. Impact of Vehicle Speed

We repeated the above tests under different vehicle speeds: 10 mph (4.5 m/s), 15 mph (6.7 m/s), 20 mph (8.9 m/s), and 30 mph (13.4 m/s). Unfortunately, we were not allowed to test at a higher speed due to the speed limit. We conducted 20 tests for each case. In our tests, the antenna spacing was 5 ft and the phone was on driver's left ear.

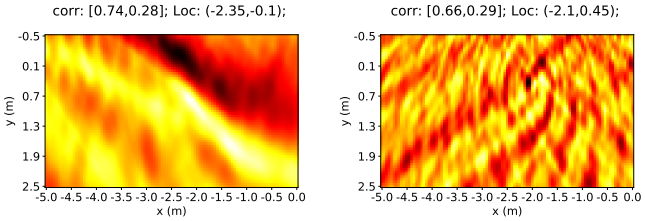

(a) 2 ft antenna spacing. (b) 3 ft antenna spacing.

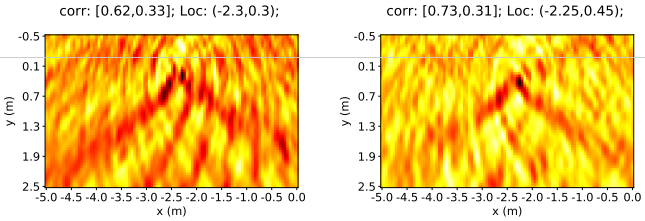

(c) 4 ft antenna spacing. (d) 5 ft antenna spacing.

Fig. 17: Inverse correlation heatmap generated by PhoLoc when it uses different antenna spacings.

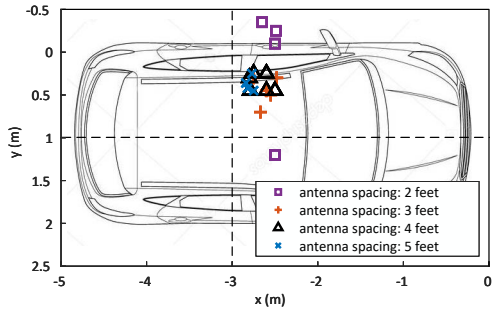

Fig. 18: The estimated phone location when PhoLoc uses different antenna spacings.

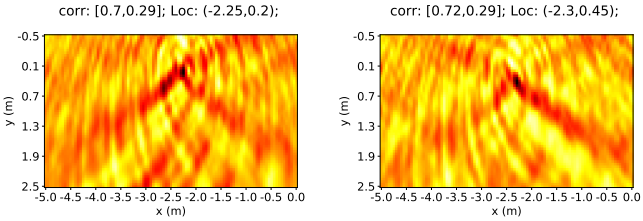

(a) 10 mph speed. (b) 15 mph speed.

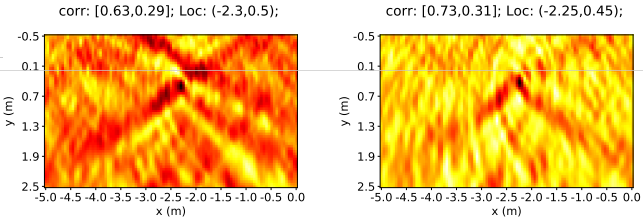

(c) 20 mph speed. (d) 30 mph speed.

Fig. 19: Inverse correlation heatmap generated by PhoLoc when the vehicle drives at different speeds.

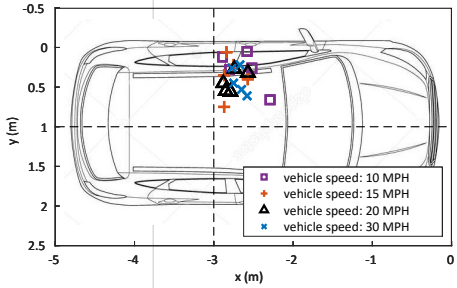

Fig. 20: PhoLoc's results when vehicle is driving at different speeds.

Fig. 19 shows an example of inverse heatmap for each case. Fig. 20 shows the results of first five tests in each case. Of all the tests, the standard deviation of $(\Delta x, \Delta y)$ is (0.24, 0.24) in the 10 mph case, (0.12, 0.25) in the 15 mph case, (0.12, 0.13) in the 20 mph case, and (0.07, 0.14) in the 30 mph case. Two observations could be made based on the experimental results: i) PhoLoc performs well at all tested vehicle speeds; and ii) a high vehicle speed tends to offer a better performance. The second observation can be attributed to the fact that, in practice, vehicle speed is more stable at a higher speed. That is, a/v decreases as v increases, where v is vehicle speed and a is vehicle acceleration.

F. Impact of Driver's Phone-Holding Style

In this study, we repeat the above experiments when the driver is on a voice phone call. We consider three cases: i) driver holds phone on his left ear; ii) driver holds phone in front of his mouth; and iii) driver holds phone on his right ear (see Fig. 11). For each case, we conducted 20 tests. For these tests, the antenna spacing is 5 ft, and the vehicle speed is about 20 mph.

Fig. 21 shows the results of the first 10 tests in each case. Of all the tests, the standard deviation of $(\Delta x, \Delta y)$ is (0.09,0.17) when driver holds phone on his left ear, (0.13,0.10) when driver holds phone in front of his mouth, and (0.49,0.41) when driver holds phone on his right ear. Apparently, PhoLoc has the best performance when phone is in front of mouth, an acceptable performance when phone is on left ear, and a poor performance when phone is on right ear. This is because PhoLoc has a LoS path to reach phone in the first two cases while it does not have LoS path to reach phone in the third case. When a driver holds phone on his ear, his head blocks the signal, leading to a poor performance of PhoLoc.

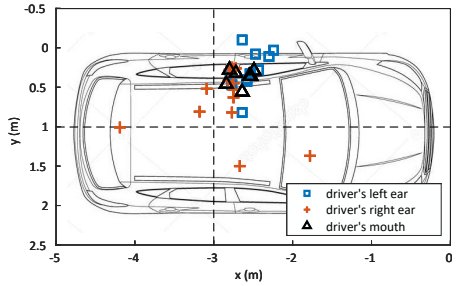

Fig. 21: PhoLoc's results when phone is held at different positions.

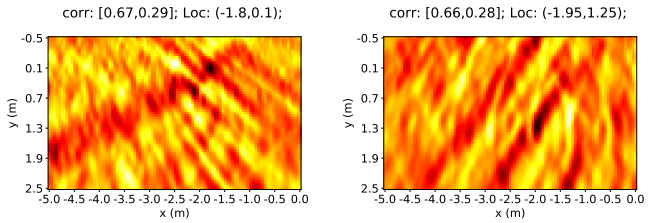

(a) Driver seat. (b) Passenger seat.

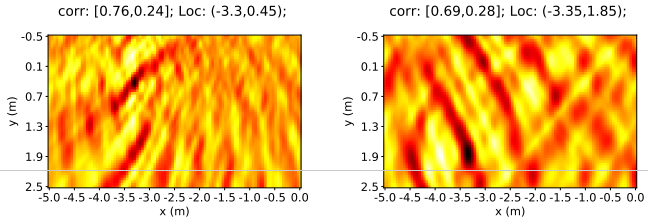

(c) Back-left seat. (d) Back-right seat.

Fig. 22: Inverse correlation heatmap generated by PhoLoc when the caller is on different seats and the caller holds phone on his left ear.

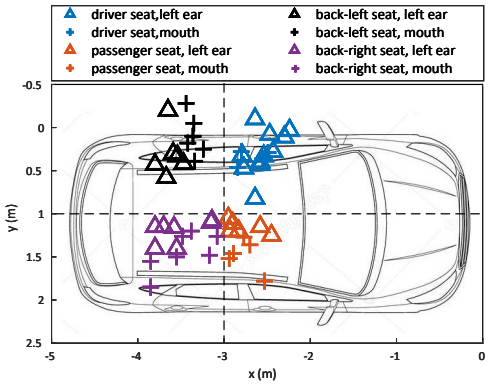

Fig. 23: PhoLoc's results when the phone call was made by a caller on different seats in a vehicle.

G. Impact of Phone Location in Vehicle

We conducted tests to evaluate the performance of PhoLoc when the caller is on different seats in a vehicle. Specifically, we considered four spots for the caller: driver seat, passenger seat, back-left seat, and back-right seat. For each case, we did 10 tests for caller's left ear, 10 tests for caller's mouth, and 10 tests for caller's right ear. The experiment setup is shown in Fig. 11. Two people were in the vehicle at the same time for these tests.

Similar to the observations in §V-F, PhoLoc performs well when phone is on caller's left ear and in front of caller's mouth, but it does not perform well when phone is on right ear. The reason is the same, i.e., when phone is on right ear, caller's head blocks the signal. A simple treatment to this issue is to deploy two PhoLoc devices on roadside: one is on vehicle's left side and the other is on vehicle's right side. Therefore, we only present the results when phone is on caller's left ear and in front of caller's mouth.

Fig. 22 shows inverse correlation heatmap from the four cases when the phone is on caller's left ear. Fig. 23 presents the results of the four cases when phone is either on caller's left ear or in front of caller's mouth. Overall, the standard deviation of $(\Delta x, \Delta y)$ is (0.15,0.18) when caller is on driver's seat, (0.21,0.21) when caller is on passenger seat, (0.11,0.19) when caller is on back-left seat, and (0.28,0.24) when caller is on back-right seat.

TABLE I: The overall performance of PhoLoc.

Driver's phone call violation detection	False positive rate	(4/96 =) 4.2%
	False negative rate	(8/58 =) 13.8%
Phone location classification	Invalid data ratio	(23/103 =) 22.3%
	Classification accuracy	(69/80 =) 86.3%

H. Extensive Experimental Results

Driver's Phone Call Violation Detection. Recall that our objective is to detect vehicle driver's phone call violation. In total, we did 58 tests for the event that a vehicle driver was on a phone call. PhoLoc made an incorrect decision for 8 of them, most of which correspond to the case of driver holding the phone on his right ear. Therefore, the false negative rate is (8/58=) 13.8%. On the other hand, we did 96 tests in total for the event that the phone call is made by a passenger (on passenger seat or back seats) rather than the driver. PhoLoc made an incorrect decision for 4 tests. Therefore, the false positive rate is (4/96) = 4.2%. Additionally, we note that, when a passenger holds phone on his right ear, the resulting correlation value in Equation (14) is typically less than the threshold ($c_b = 0.61$) and, therefore, PhoLoc would not make an incorrect decision for those cases. Table I summarizes the overall results of PhoLoc.

Phone/Caller In-Vehicle Location Classification. A natural extension of PhoLoc is to classify the location of an active phone caller in a vehicle: driver seat, passenger seat, back-left seat, or back-right seat. For this problem, we assume that there are two PhoLoc devices deployed on road's two sides. We use the above measurement results to infer the accuracy of position detection. Specifically, we exclude the data from the case where driver or passenger holds phone on his right ear, as this case can be handled by the other PhoLoc device. Data analysis shows that, among a total of 103 tests, 23 tests yields a correlation less than c_b (i.e., 0.61). Therefore, the invalid data rate is (23/103=) 22.3%. Among those valid measurements, the correct position was found by PhoLoc in 69 tests. So the classification accuracy is (69/80=) 86.3%. Table I summarizes our overall results.

VI. Limitations and Discussions

Computation-Efficient Algorithms. To find the relative location of a mobile phone, we formulated an optimization problem and employed brute-force search for the pursuit of its optimal solution. While brute-force search can be done in a few seconds, efficient solving algorithms are desirable. A possible approach is to disentangle the coupling of Δx, Δy, and v, so that the optimal values of these three variables can be found through a 3-dimensional FFT operation (following the idea of Omega-K algorithm [32]).

Other Violations of Phone Use. Driver's violation of phone use includes making phone call, sending text message, browsing website, and others. While PhoLoc was designed and evaluated for the detection of driver's phone call violation, it can also be used to detect other phone use violations. For example, the intermittent signal transmission of a phone will last for seconds when sending a single text message. The phone signals can be collected and processed in the same way as we presented to classify the phone location in a vehicle and detect the driver's violation of phone use. In our future work, we will use the radio signals emitted by a phone to: i) classify its user's activities (e.g., texting, web browsing, and listening to music), and ii) estimate its relative location in a vehicle. Based on the classification and estimation results, we will design a learning-based approach to determine if there is a violation of phone use in a vehicle.

Vehicle-Dense Scenarios. In the scenarios where a road has dense vehicles, the LoS path between PhoLoc and a target vehicle might be blocked by another vehicle. In this case, a single PhoLoc detector may not work well due to the inaccurate distance measurement of its lidar sensor. Given the short time duration of lidar's effective measurement (less than 1 s) for a vehicle, this problem can be alleviated by deploying multiple PhoLoc detectors on both sides of a road. We anticipate that increasing the number of PhoLoc detectors on roadsides will significantly increase the accuracy of detecting a vehicle driver's violation of phone use.

Error Sources. The primary sources of localization error in our system can be attributed to several factors: *(i) Inaccurate Radio Frequency*: The frequency utilized by PhoLoc to estimate radio signal wavelength is an average from multiple subcarriers. The carrier frequency of radio signal is an estimation and not accurate. *(ii) Variation in Vehicle Speed*: During the time period of measurement, the speed of a vehicle may not be constant. The variation of vehicle speed may contribute to the localization error of PhoLoc. *(iii) Noise and Other Imperfections*: PhoLoc implemented the proposed localization approach on an SDR testbed, which is not optimized for out-of-band interference and noise suppression. The noise and other imperfections of the SDR platform contribute to the localization error of PhoLoc. *(iv) Lidar Measurement Error*: Variations in lidar measurements of y_s due to vehicle movement, along with the averaging of y_s from continuous measurements, is another source of PhoLoc's localization error.

VII. Related Work

We review the related work in two areas: distracted driving detection and wireless localization.

Camera-Based Distracted Driving Detection. Camera, together with AI-based computer vision techniques, has been widely studied to monitor vehicle driver's status and detect his/her violation of phone use [33], [4], [34], [35], [36], [37], [38], [7], [39]. However, most of these works require the camera to be installed inside a vehicle. Therefore, the proposed camera-based detection systems are mainly limited to private use (e.g., commercial vehicles). Recently, deploying high-resolution cameras on road side to detect distracted drivers has emerged as a new approach to enforce driving-safety-related laws [2]. Some countries such as UK and Austria have experimented this approach and demonstrated its feasibility in practice [2]. Despite the recent advances in computer vision, camera-based approaches may not work well in some scenarios (e.g., darkness and bad weather condition) and may raise privacy concerns.

Phone Monitoring While Driving. In addition to cameras, other sensors (e.g., smartphone's accelerometers and gyroscopes) have been studied to limit drivers' phone use in unsafe conditions and improve driving safety [40], [41], [6], [5]. PhoLoc differs and complements the results along this research line. In particular, [42] presents a roadside radio device that detects a vehicle driver's phone use by analyzing the overheard radio signals from a phone. However, it is impossible for this approach to figure out if the phone call is made by a driver or someone else in vehicle.

WiFi Localization. Another research line closely related to our work is wireless localization, which has generated many results in the past two decades. Particularly, wireless localization has been intensively studied in 802.11 networks to localize a WiFi device [14], [15], [16], [17], [18], [19], [43]. Most of these works rely on the acquisition of CSI to estimate the AoA (angle-of-arrival) and/or ToF (time-of-flight) of the signals from a target device. The estimated AoA and/or ToF information is then used to infer the location of the target device. These approaches, however, only work for a stationary or semi-stationary target device. They cannot apply to our localization problem for two additional reasons: i) PhoLoc does not have CSI; and ii) PhoLoc has only one radio receiver.

Cellular Localization. Phone localization has been studied and developed as a function of cellular networks to enable location-based applications and public safety services. Features used for phone localization in cellular networks include cell proximity, signal strength, AoA, time of arrival (TOA), time difference of arrival (TDOA) [44]. Recently, machine learning has been applied to phone localization in cellular networks and achieved sub-meter accuracy in some test scenarios [45], [46], [47], [48]. However, given the nature of its large scale, cellular localization cannot achieve the required accuracy of PhoLoc, let alone estimating phone's relative location in a vehicle.

Near-Field Localization. Research on near-field source localization has been around for many years, at least dating back to 1990s [49]. However, existing works focus on localizing stationary device and remain in theoretical study [50], [51], [52]. In contrast, PhoLoc considers a moving device and focuses on its practical realization.

VIII. Conclusion

This paper focuses on the design of a roadside sensing device for transportation infrastructure to improve driving safety by taking advantage of recent advances in wireless technologies. It presented a roadside device called PhoLoc to detect the violation of driver's phone use in personal vehicles. PhoLoc is made of two distinct sensors: radio and lidar. It jointly processes the multi-modal data from the two sensors to

estimate the relative phone location in a vehicle. The novelty of PhoLoc is a near-field localization scheme, which is capable of estimating the location of a mobile device at a specific time moment by overhearing its radio signals. We have built a prototype of PhoLoc and evaluated its performance in realistic scenarios. Experimental results show that PhoLoc achieves 4.2% false positive rate and 13.8% false negative rate in the detection of driver's phone call violation.

REFERENCES

[1] National Highway Traffic Safety Administration (NHTSA), "Traffic safety facts research note." https://tinyurl.com/ypdctc6c, 2023. online [Accessed: 29-September-2023].

[2] V. Shah, "Mobile phone detection cameras: How do they work?." https://tinyurl.com/yc7vzvv6, November 2021. [Online; accessed 29-September-2023].

[3] C. Bo, X. Jian, X.-Y. Li, X. Mao, Y. Wang, and F. Li, "You're driving and texting: detecting drivers using personal smart phones by leveraging inertial sensors," in *Proceedings of the 19th annual international conference on Mobile computing & networking*, pp. 199–202, 2013.

[4] C. Streiffer, R. Raghavendra, T. Benson, and M. Srivatsa, "Darnet: a deep learning solution for distracted driving detection," in *Proceedings of the 18th acm/ifip/usenix middleware conference: Industrial track*, pp. 22–28, 2017.

[5] K. B. Ahmed, B. Goel, P. Bharti, S. Chellappan, and M. Bouhorma, "Leveraging smartphone sensors to detect distracted driving activities," *IEEE Transactions on Intelligent Transportation Systems*, vol. 20, no. 9, pp. 3303–3312, 2018.

[6] L. Jiang, X. Lin, X. Liu, C. Bi, and G. Xing, "Safedrive: Detecting distracted driving behaviors using wrist-worn devices," *Proceedings of the ACM on Interactive, Mobile, Wearable and Ubiquitous Technologies*, vol. 1, no. 4, pp. 1–22, 2018.

[7] A. Kashevnik, I. Lashkov, A. Ponomarev, N. Teslya, and A. Gurtov, "Cloud-based driver monitoring system using a smartphone," *IEEE Sensors Journal*, vol. 20, no. 12, pp. 6701–6715, 2020.

[8] J. Wahlström, I. Skog, P. Händel, B. Bradley, S. Madden, and H. Balakrishnan, "Smartphone placement within vehicles," *IEEE transactions on intelligent transportation systems*, vol. 21, no. 2, pp. 669–679, 2019.

[9] H. Jiang, J. Hu, D. Liu, J. Xiong, and M. Cai, "Driversonar: Fine-grained dangerous driving detection using active sonar," *Proceedings of the ACM on Interactive, Mobile, Wearable and Ubiquitous Technologies*, vol. 5, no. 3, pp. 1–22, 2021.

[10] F. Wang, J. Liu, and W. Gong, "Multi-adversarial in-car activity recognition using rfids," *IEEE Transactions on Mobile Computing*, vol. 20, no. 6, pp. 2224–2237, 2020.

[11] C. Yang, X. Wang, and S. Mao, "Respiration monitoring with rfid in driving environments," *IEEE Journal on Selected Areas in Communications*, vol. 39, no. 2, pp. 500–512, 2020.

[12] C. Yang, X. Wang, and S. Mao, "Unsupervised drowsy driving detection with rfid," *IEEE transactions on vehicular technology*, vol. 69, no. 8, pp. 8151–8163, 2020.

[13] S. Ragot, B. Kovesi, R. Trilling, D. Virette, N. Duc, D. Massaloux, S. Proust, B. Geiser, M. Gartner, S. Schandl, *et al.*, "Itu-t g. 729.1: An 8-32 kbit/s scalable coder interoperable with g. 729 for wideband telephony and voice over ip," in *2007 IEEE International Conference on Acoustics, Speech and Signal Processing-ICASSP'07*, vol. 4, pp. IV–529, IEEE, 2007.

[14] M. Kotaru, K. Joshi, D. Bharadia, and S. Katti, "Spotfi: Decimeter level localization using wifi," in *Proceedings of the 2015 ACM Conference on Special Interest Group on Data Communication*, pp. 269–282, 2015.

[15] J. Xiong and K. Jamieson, "{ArrayTrack}: A {Fine-Grained} indoor location system," in *10th USENIX Symposium on Networked Systems Design and Implementation (NSDI 13)*, pp. 71–84, 2013.

[16] Y. Xie, J. Xiong, M. Li, and K. Jamieson, "xd-track: leveraging multi-dimensional information for passive wi-fi tracking," in *Proceedings of the 3rd Workshop on Hot Topics in Wireless*, pp. 39–43, 2016.

[17] Y. Xie, J. Xiong, M. Li, and K. Jamieson, "md-track: Leveraging multi-dimensionality for passive indoor wi-fi tracking," in *The 25th Annual International Conference on Mobile Computing and Networking*, pp. 1–16, 2019.

[18] E. Soltanaghaei, A. Kalyanaraman, and K. Whitehouse, "Multipath triangulation: Decimeter-level wifi localization and orientation with a single unaided receiver," in *Proceedings of the 16th annual international conference on mobile systems, applications, and services*, pp. 376–388, 2018.

[19] J. Xiong, K. Sundaresan, and K. Jamieson, "Tonetrack: Leveraging frequency-agile radios for time-based indoor wireless localization," in *Proceedings of the 21st Annual International Conference on Mobile Computing and Networking*, pp. 537–549, 2015.

[20] R. J. Selina, E. J. Murphy, M. McKinnon, A. Beasley, B. Butler, C. Carilli, B. Clark, A. Erickson, W. Grammer, J. Jackson, *et al.*, "The next-generation very large array: a technical overview," in *Ground-based and Airborne Telescopes VII*, vol. 10700, p. 107001O, International Society for Optics and Photonics, 2018.

[21] S. Coleri, M. Ergen, A. Puri, and A. Bahai, "Channel estimation techniques based on pilot arrangement in ofdm systems," *IEEE Transactions on broadcasting*, vol. 48, no. 3, pp. 223–229, 2002.

[22] A. Ilumba, "The 3g shut down: Will your phone be affected?." https://tinyurl.com/3wvdpfas, Accessed:29-September-2023.

[23] "What are the cellular frequencies of carriers in usa & canada?." https://tinyurl.com/2hb5429r, Accessed:29-September-2023.

[24] A. Yonis, M. Abdullah, and M. Ghanim, "Lte-fdd and lte-tdd for cellular communications," *Proceeding, Progress in*, 2012.

[25] B. Goode, "Voice over internet protocol (voip)," *Proceedings of the IEEE*, vol. 90, no. 9, pp. 1495–1517, 2002.

[26] C. C. Expert, "Voip packet size and packet rate examples." https://tinyurl.com/4dptbyv2, Accessed:11-September-2023.

[27] H. Holma and A. Toskala, *LTE for UMTS: OFDMA and SC-FDMA based radio access*. John Wiley & Sons, 2009.

[28] E. Yaacoub and Z. Dawy, "A survey on uplink resource allocation in ofdma wireless networks," *IEEE Communications Surveys & Tutorials*, vol. 14, no. 2, pp. 322–337, 2011.

[29] MakerFocus, "Makerfocus tfmini-s micro lidar module." https://tinyurl.com/2wbre64b, Accessed:29-September-2023.

[30] E. Blossom, "Gnu outoftreemodules." https://wiki.gnuradio.org/index.php/OutOfTreeModules, Accessed:29-September-2023.

[31] "Gnu radio." https://www.gnuradio.org, Accessed:29-September-2023.

[32] S. Wu, H. Wang, C. Li, X. Liu, and G. Fang, "A modified omega-k algorithm for near-field single-frequency mimo-arc-array-based azimuth imaging," *IEEE Transactions on Antennas and Propagation*, vol. 69, no. 8, pp. 4909–4922, 2021.

[33] B. Wagner, F. Taffner, S. Karaca, and L. Karge, "Vision based detection of driver cell phone usage and food consumption," *IEEE transactions on intelligent transportation systems*, vol. 23, no. 5, pp. 4257–4266, 2021.

[34] Y. Xing, C. Lv, H. Wang, D. Cao, E. Velenis, and F.-Y. Wang, "Driver activity recognition for intelligent vehicles: A deep learning approach," *IEEE transactions on Vehicular Technology*, vol. 68, no. 6, pp. 5379–5390, 2019.

[35] C. Huang, X. Wang, J. Cao, S. Wang, and Y. Zhang, "Hcf: a hybrid cnn framework for behavior detection of distracted drivers," *IEEE access*, vol. 8, pp. 109335–109349, 2020.

[36] R. Khurana and M. Goel, "Eyes on the road: Detecting phone usage by drivers using on-device cameras," in *Proceedings of the 2020 CHI Conference on Human Factors in Computing Systems*, pp. 1–11, 2020.

[37] R. A. Berri, A. G. Silva, R. S. Parpinelli, E. Girardi, and R. Arthur, "A pattern recognition system for detecting use of mobile phones while driving," in *2014 International Conference on Computer Vision Theory and Applications (VISAPP)*, vol. 2, pp. 411–418, IEEE, 2014.

[38] K. Seshadri, F. Juefei-Xu, D. K. Pal, M. Savvides, and C. P. Thor, "Driver cell phone usage detection on strategic highway research program (shrp2) face view videos," in *Proceedings of the IEEE Conference on Computer Vision and Pattern Recognition Workshops*, pp. 35–43, 2015.

[39] J. Liang, H. Zhu, E. Zhang, and J. Zhang, "Stargazer: A transformer-based driver action detection system for intelligent transportation," in *Proceedings of the IEEE/CVF Conference on Computer Vision and Pattern Recognition*, pp. 3160–3167, 2022.

[40] Y. Wang, J. Yang, H. Liu, Y. Chen, M. Gruteser, and R. P. Martin, "Sensing vehicle dynamics for determining driver phone use," in *Proceeding of the 11th annual international conference on Mobile systems, applications, and services*, pp. 41–54, 2013.

[41] C. Jiang, Y. He, X. Zheng, and Y. Liu, "Orientation-aware RFID tracking with centimeter-level accuracy," in *17th ACM/IEEE International Conference on Information Processing in Sensor Networks (IPSN)*, pp. 290–301, IEEE, 2018.

[42] T. M. Brennan Jr, J. E. Jesson, and P. G. A. Furlanetto, "Quantifying driver cell phone use at signalized intersections using software-defined radio," *Traffic injury prevention*, vol. 20, no. 4, pp. 359–364, 2019.
[43] T.-C. Tai, K. C.-J. Lin, and Y.-C. Tseng, "Toward reliable localization by unequal aoa tracking," in *Proceedings of the 17th Annual International Conference on Mobile Systems, Applications, and Services*, pp. 444–456, 2019.
[44] C. Laoudias, A. Moreira, S. Kim, S. Lee, L. Wirola, and C. Fischione, "A survey of enabling technologies for network localization, tracking, and navigation," *IEEE Communications Surveys & Tutorials*, vol. 20, no. 4, pp. 3607–3644, 2018.
[45] H. Rizk, M. Torki, and M. Youssef, "Cellindeep: Robust and accurate cellular-based indoor localization via deep learning," *IEEE Sensors Journal*, vol. 19, no. 6, pp. 2305–2312, 2018.
[46] A. Chakraborty, L. E. Ortiz, and S. R. Das, "Network-side positioning of cellular-band devices with minimal effort," in *2015 IEEE Conference on Computer Communications (INFOCOM)*, pp. 2767–2775, IEEE, 2015.
[47] H. Zang, F. Baccelli, and J. Bolot, "Bayesian inference for localization in cellular networks," in *2010 Proceedings IEEE INFOCOM*, pp. 1–9, IEEE, 2010.
[48] A. Ray, S. Deb, and P. Monogioudis, "Localization of lte measurement records with missing information," in *IEEE INFOCOM 2016-The 35th Annual IEEE International Conference on Computer Communications*, pp. 1–9, IEEE, 2016.
[49] Y.-D. Huang and M. Barkat, "Near-field multiple source localization by passive sensor array," *IEEE Transactions on antennas and propagation*, vol. 39, no. 7, pp. 968–975, 1991.
[50] Y. Wang and K. Ho, "Unified near-field and far-field localization for aoa and hybrid aoa-tdoa positionings," *IEEE Transactions on Wireless Communications*, vol. 17, no. 2, pp. 1242–1254, 2017.
[51] J. He, M. O. Ahmad, and M. Swamy, "Near-field localization of partially polarized sources with a cross-dipole array," *IEEE Transactions on Aerospace and Electronic Systems*, vol. 49, no. 2, pp. 857–870, 2013.
[52] B. Friedlander, "Localization of signals in the near-field of an antenna array," *IEEE Transactions on Signal Processing*, vol. 67, no. 15, pp. 3885–3893, 2019.

Shichen Zhang is currently a Ph.D. student in the Department of Computer Science and Engineering at Michigan State University (MSU), East Lansing, MI. He received his B.Eng. degree in Automation from Beijing University of Technology, Beijing, China, in 2018 and M.Eng. degree in Electrical and Computer Engineering from Cornell University, Ithaca, NY, in 2019. His current research interests focus on wireless networks, sensing systems, and deep learning.

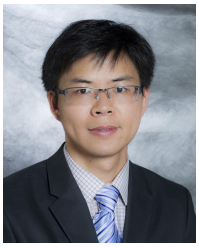

Huacheng Zeng (SM'20) received a Ph.D. degree in Computer Engineering from Virginia Polytechnic Institute and State University (Virginia Tech), Blacksburg, VA. He is currently an Assistant Professor in the Department of Computer Science and Engineering at Michigan State University (MSU), East Lansing, MI. Prior to joining MSU, he was an Assistant Professor of Electrical and Computer Engineering at the University of Louisville, Louisville, KY, and a Senior System Engineer at Marvell Semiconductor, Santa Clara, CA. He is a recipient of the NSF CAREER Award in 2019. He received the Best Paper Award from IEEE SECON 2021 and ACM WUWNet 2014. His research interest is broadly in wireless networking and sensing systems.

Y. Thomas Hou (F'14) received his Ph.D. from NYU Tandon School of Engineering in 1998. He is currently Bradley Distinguished Professor of Electrical and Computer Engineering at Virginia Tech, Blacksburg, VA, USA, which he joined in 2002. He was a Member of Research Staff at Fujitsu Laboratories of America in Sunnyvale, CA from 1997 to 2002. His current research focuses on developing real-time optimal solutions to complex science and engineering problems arising from wireless and mobile networks. He is also interested in wireless security. He has published over 350 papers in IEEE/ACM journals and conferences. His papers were recognized by 10 best paper awards from IEEE and ACM, including an IEEE INFOCOM Test of Time Paper Award in 2023. He holds six U.S. patents. He authored/co-authored two graduate textbooks: *Applied Optimization Methods for Wireless Networks* (Cambridge University Press, 2014) and *Cognitive Radio Communications and Networks: Principles and Practices* (Academic Press/Elsevier, 2009). Prof. Hou was named an IEEE Fellow for contributions to modeling and optimization of wireless networks. He was/is on the editorial boards of a number of IEEE and ACM transactions and journals. He was Steering Committee Chair of IEEE INFOCOM conference and was a member of the IEEE Communications Society Board of Governors. He was also a Distinguished Lecturer of the IEEE Communications Society.